# Scaling crossovers in activated escape of nonequilibrium systems: a resonantly driven oscillator.

Oleg Kogan*
*Caltech, Pasadena CA*
(Dated: October 22, 2008)

The rate of metastable decay in nonequilibrium systems is expected to display scaling behavior: i.e., the logarithm of the decay rate should scale as a power of the distance to a bifurcation point where the metastable state disappears. Recently such behavior was observed and some of the earlier predicted exponents were found in experiments on several types of systems described by a model of a modulated oscillator. Here we establish the range where different scaling behavior is displayed and show how the crossover between different types of scaling occurs. The analysis is done for a nonlinear oscillator with two coexisting stable states of forced vibrations. Our numerical calculations, based on the the instanton method allow the mapping of the entire parameter range of bi-stability. We find the regions where the scaling exponents are 1 or 3/2, depending on the damping. The exponent 3/2 is found to extend much further from the bifurcation then were it would be expected to hold as a result of an over-damped soft mode. We also uncover a new scaling behavior with exponent of $\approx$ 1.3 which extends, numerically, beyond the close vicinity of the bifurcation point.

PACS numbers:



## I. INTRODUCTION

The problem of noise-induced escape from a metastable state has been studied in various contexts, from nucleation to chemical reactions to switching in nanomagnets. The escape rate often has the Arrhenius form $W \propto \exp(-R/D)$, where $D$ is the noise intensity (temperature, in the case of thermal noise). Of central interest both for theory and experiment is the activation energy $R$. Starting with the Kramers paper [1] much work has been put into calculating $R$ and the prefactor in the escape rate for various physical systems. From this point of view, it is particularly important to reveal generic features of the activation energy $R$, such as scaling behavior with the system parameters. The onset of the scaling behavior was noticed first for systems close to thermal equilibrium [2, 3]. Scaling occurs also for systems far from thermal equilibrium, which generally do not have detailed balance [4, 5, 6, 7, 8]. Nonequilibrium systems may display several types of scaling behaviors and crossovers between different scalings with varying system parameters.

A nonequilibrium system that has attracted much attention recently is a Duffing oscillator modulated by a periodic force

$$\ddot{q} + 2\Gamma\dot{q} + \omega_0^2 q + \gamma q^3 = A\cos(\omega_F t) + f(t) \qquad (1)$$

with high quality factor $\mathcal{Q} = \frac{\omega_0}{2\Gamma}$. The term $f$ is white noise with property $\langle f(t)f(t')\rangle = 2B\delta(t-t')$. As a result of the modulation the oscillator may have two or more coexisting states of forced vibrations. Noise leads to switching between these states. In this paper we will use the following two parameters: dimensionless friction, $\Omega^{-1} = \Gamma/|\omega_F - \omega_0|$ and a dimensionless driving strength, $\sqrt{\beta} = A\sqrt{3\gamma/32\omega_F^3|\omega_F-\omega_0|^3}$. In the space of $\sqrt{\beta}$ and $\Omega^{-1}$, the region of bi-stability is closed (Fig. 1).

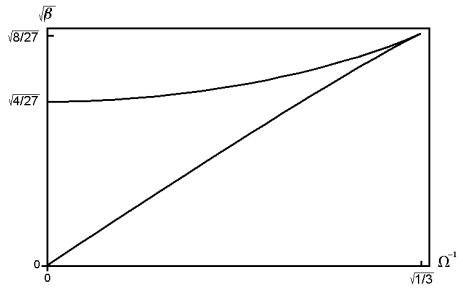


FIG. 1: Region of bi-stability in the parameter space of the driving, $\sqrt{\beta}$ and friction, $\Omega^{-1}$.

Upon varying $\sqrt{\beta}$ at a fixed $\Omega$ one would encounter an amplitude response curve such as that depicted in Fig. 2, which exhibits a region of bi-stability between two bifurcation points $\sqrt{\beta_B^l}$ and $\sqrt{\beta_B^h}$. It is critically important to note that at any finite $\Omega^{-1}$, bi-stability will exist only at a non-zero $\beta$. Therefore the problem of transition rates between two stable attractors is a *non-equilibrium* problem!

Several types of scaling behavior of the switching activation energy have been seen for such different systems as modulated nanoelectromechanical (NEMS) [10, 11, 16], and microelectromechanical (MEMS) oscillators [13] (various sources of noise in the nanomechanical systems have been thoroughly described in [9]), Josephson junctions [14], optically trapped atoms [15], and superconducting resonators [17] - all of these systems are modelled as Duffing oscillators. Not only is this scaling interesting on its own, but it also underlies various applications, an important example being quantum measurements [14].

*Electronic address: oleg@caltech.edu

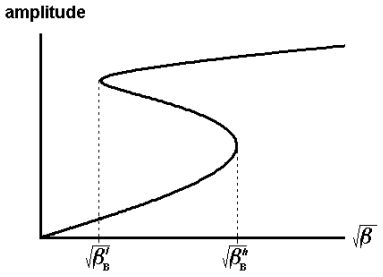


FIG. 2: Amplitude versus $\sqrt{\beta}$ for some given $\Omega^{-1} \neq 0$. The upper and lower branches corresponds to a stable steady state, while the middle branch corresponds to a steady state which is unstable with respect to small perturbations. Similar curve exists for *phase* versus $\sqrt{\beta}$. A bifurcation value of $\sqrt{\beta}$ will be denoted by $\sqrt{\beta_B}$; there are two of these: $\sqrt{\beta_B^h}$ and $\sqrt{\beta_B^l}$. Noise-induced transitions from low amplitude to high amplitude branch will be called "down $\rightarrow$ up transitions", and those from high amplitude to low amplitude branch, will be called "up $\rightarrow$ down transitions".

Let $\tilde{\eta} = \left|\sqrt{\beta} - \sqrt{\beta_B}\right|$ (the letter $\eta$ is reserved for denoting $\beta - \beta_B$ in recent work by one of the authors, see [26] for example). In certain cases, the switching activation energy obeys a power law: $R \sim \tilde{\eta}^{\xi}$. There exist regimes when the escape problem can be reduced to that of escape over a 1-dimensional potential barrier. Analytical approximations are valid in two such regimes - close to bifurcation points, where $\xi = 3/2$ and at at low $\Omega^{-1}$, where $\xi = 1$ are summarized in Section II.A. A new *geometric* explanation of these $\xi = 3/2$ and $\xi = 1$ exponents has recently been given [27]. These authors make use of a remarkable feature of this system - that the bifurcation at $\sqrt{\beta_B^l}$ is "non-local" while the bifurcation at $\sqrt{\beta_B^h}$ is "local", as will be explained in Section II.B.

In this paper we present a detailed theoretical study of the scaling and scaling crossovers of the activation energy for a Duffing oscillator. Using numerical techniques, we map out the entire bi-stability region shown in Fig. 1. We identify part of this bi-stability region where the $\xi = 3/2$ and $\xi = 1$ scaling laws hold, where there are crossovers between these scaling laws, as well as regions of other scaling behaviors not previously mentioned in the literature.

## II. BRIEF REVIEW OF EXISTING THEORY

We will analyze the system in the canonically transformed phase space $(Q, P)$, with $q = 2^{3/2}\omega_0\sqrt{\frac{|\omega_0-\omega_F|}{3\gamma}}\left(Q\cos\left(\omega_F t\right) + P\sin\left(\omega_F t\right)\right)$ and $\dot{q} = 2^{3/2}\omega_F\omega_0\sqrt{\frac{|\omega_0-\omega_F|}{3\gamma}}\left(-Q\sin\left(\omega_F t\right) + P\cos\left(\omega_F t\right)\right)$. In the underdamped limit when $\mathcal{Q} \gg 1$, the motion of $q$ is approximately simple-harmonic, with slow "envelope" evolution represented by $P$ and $Q$. The resulting equations for $P$ and $Q$ are approximately independent of time - the fast time-dependent corrections average to zero to lowest order in $\mathcal{Q}^{-1}$. In terms of slow time $T \equiv \mathcal{Q}^{-1}t$ (subsequently, the dot denoting $d/dT$), it follows the following evolution [28]:

$$\dot{Q} = K_Q(Q,P) + n_Q(T) \tag{2}$$

$$\dot{P} = K_P(Q,P) + n_P(T) \tag{3}$$

where $K_Q(Q,P) = \frac{\partial g}{\partial P} - \Omega^{-1}Q$ and $K_P(Q,P) = -\frac{\partial g}{\partial Q} - \Omega^{-1}P$, $g(Q,P)$ is a Hamiltonian given by $g = \frac{1}{4}(Q^2+P^2-1)^2 - \sqrt{\beta}Q$ and $\Omega^{-1}$ is an effective damping which tends to arrest the amplitude to zero. The $n_i$s are stochastic terms which will be modelled as white noise: $\langle n_i(T)n_j(T')\rangle = 2D\delta_{ij}\delta(T-T')$ where $D = \left(\frac{3\gamma B}{16\omega_F^3\Gamma^2}\right)\Omega^{-2}$. The terms inside (...) have been defined on the first page and are all parameters of the oscillator. In the absence of noise, an initial condition $(Q_0, P_0)$ will evolve into one of the two attracting fixed points (FP), or "attractors". The third FP is of saddle type - its amplitude forms the middle branch in Fig. 2. The separatrix between the basins of attraction of each of the two attractors is a set of initial conditions that flows into the saddle FP via its attractive eigen-direction.

In the presence of noise, an initial condition $(Q_0, P_0)$ follows a continuous random walk in the deterministic flow $\vec{K}$. The probability density (PDF) $\rho(x,y)$ of reaching $(Q,P)$ from some initial $(Q_0,P_0)$ satisfies the Fokker-Plank equation (FPE): $\frac{\partial\rho}{\partial T} - \{g,\rho\} = \vec{\nabla}\cdot\left(\Omega^{-1}\vec{r}\rho + D\vec{\nabla}\rho\right)$. The solution can be written as a functional integral of $\exp\left[-\frac{1}{D}\int_{(Q_0,P_0)}^{(Q,P)}\mathcal{L}\left(Q'(T),P'(T)\right)dT\right]$ over all paths [18], where $\mathcal{L} = \frac{1}{4}\left[\left(\dot{Q}-K_Q\right)^2 + \left(\dot{P}-K_P\right)^2\right]$. One can re-express all paths as variations around the optimal path that minimizes the exponent. Then $\rho(Q,P) = \rho'(Q,P)\exp\left[-\frac{1}{D}min\int_{(Q_0,P_0)}^{(Q,P)}\mathcal{L}\left(Q'(t),P'(T)\right)dT\right] = \rho'(Q,P)\exp\left[-S(Q,P)/D\right]$ where the prefactor $\rho'(Q,P)$ comes from performing path integrals over variations around the optimal path. This pre-factor is *nonexponential* because the path integral over variations is to the lowest order a Gaussian path integral. We are interested in the exponential factor, because in the limit of weak noise it will dominate transition rates.

Now, the probability of undergoing a large fluctuation from a FP to cross the separatrix is proportional to the probability of being found in the most likely place where the exit traffic takes place - the saddle point $(Q_s, P_s)$ [18]. Therefore, the rate of escape $W$ is to be approximated by $\rho(Q_s, P_s)$. To calculate the probability of escape up to this accuracy, we need in principle to solve Euler-Lagrange equations to find a path that leads from the attractor to the saddle and evaluate the action $S^*$ along this path. The Hamiltonian associated with $\mathcal{L}$ is

$$\mathcal{H} = \left(p_Q^2 + p_P^2\right) + p_Q K_Q + p_P K_P \tag{4}$$

$\mathcal{H}$ is often called the "auxiliary" Hamiltonian, to avoid confusion with $g$. The points $(Q_{FP}, P_{FP}, P_Q = 0, P_P = 0)$ are fixed points of the auxiliary dynamical system formed from $\mathcal{H}$. Let's note that there are infinitely many *optimal* trajectories from attractor to the saddle - they all differ by their initial momenta, but only paths that have zero energy give the *stationary* $\rho(Q,P)$. One way to see this is to substitute $\rho(Q,P) = \rho'(Q,P)\exp(-S(Q,P)/D)$ into the *stationary* FPE, and obtain [22] $\left(\frac{\partial S}{\partial Q}\right)^2 + \left(\frac{\partial S}{\partial P}\right)^2 + \frac{\partial S}{\partial Q}K_Q + \frac{\partial S}{\partial P}K_P = 0$. This is just a Hamilton-Jacobi equation, $\mathcal{H}(Q,P,\frac{\partial S}{\partial Q},\frac{\partial S}{\partial P}) = 0$, and it describes dynamics on the $\mathcal{H} = 0$ manifold. Now, since $\vec{K}(Q_{FP}, P_{FP}) = 0$, the momenta at all the FPs must also be zero.

In summary, in the limit of weak noise, the rate of escape $W \approx \exp(-R/D)$ where $R = S^*$ - the action along the trajectory which connects the attractor to the saddle and satisfies $\mathcal{H} = 0$.

### A. Analytical Limits

Both limits discussed below are physically analogous to the two types of limits considered by Kramers [1]: an overdamped limit and a low damping limit. One major difference is that our Hamiltonian $g(Q,P)$ does not have an explicit separation of kinetic and potential energies.

#### 1. *Overdamped regime in the vicinity of a bifurcation.*

At either $\sqrt{\beta_B^l}$ or $\sqrt{\beta_B^h}$, the saddle and one of the attracting nodes of $\vec{K}$ merge together at $(Q_B, P_B)$ in a saddle-node bifurcation. As $\sqrt{\beta}$ approaches $\sqrt{\beta_B}$, a saddle and a node approach each other, the attractive eigenvector of the saddle, and one of the attracting eigenvectors of the node align parallel to each other, and the corresponding attracting eigenvalues of both FP approach the same negative value. Also, the repulsive eigenvector of the saddle and the other attracting eigenvector of the node become equal and the corresponding eigenvalues both tend to zero. This process is depicted in the cartoon in Fig. 3.

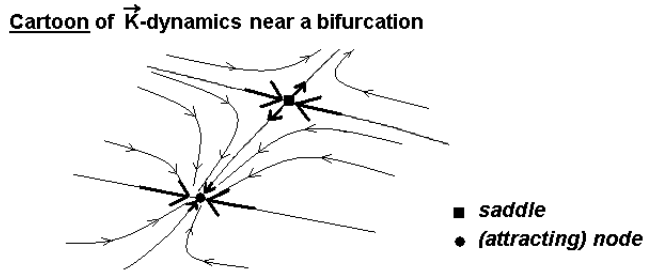


FIG. 3: Cartoon of the $\vec{K}$-flow near a saddle-node bifurcation.

Thus, close to a bifurcation, there develops a soft mode - a narrow region connecting the saddle with an attractor along which the $\vec{K}$-motion is slow. Due to this slowing down, the soft mode forms a path of least resistance along which a large noise-induced fluctuation away from the attractor is most likely to take place. To analyze this system we rewrite $\vec{K}$ in terms of parameter $\tilde{\eta}$ and variables $(f = Q - Q_B, s = P - P_B)$; it turns out to be unnecessary to make a linear transformation to eigencoordinates of $\vec{K}$ at $(Q_B, P_B, \sqrt{\beta_B})$. In terms of these new coordinates, $\vec{K}$ transforms to the following form:

$$\dot{f} = -2\Omega^{-1}(f - a_B s) + P_B f^2 + 2Q_B sf + 3P_B s^2 + f^2 s + s^3 + n_Q \quad (5)$$

$$\dot{s} = \pm\tilde{\eta} - 3Q_B f^2 - 2P_B fs - Q_B s^2 - f^3 - s^2 f + n_P \quad (6)$$

Here the + sign applies for the low field (high amplitude) bifurcation and

$$a_B = \Omega(1 \pm 2\sqrt{1 - 3\Omega^{-2}})/3. \quad (7)$$

Notice that the position of fixed points sets characteristic scaling of both $s$ and $f$ variables to be $\propto \tilde{\eta}^{1/2}$. From this we see that $s$ is a slow variable while $f$ is fast - on its time scale, $s$ appears approximately frozen. To lowest order in $\tilde{\eta}$, we treat $s$ as completely frozen, in which case $f$ relaxes to $a_B s +$corrections of order $\tilde{\eta}$. In such adiabatic limit, the dynamics of $s$ is then given by

$$\dot{s} \approx \pm\tilde{\eta} - b(\Omega)s^2 + n_P \quad (8)$$

where

$$b(\Omega) = 3Q_B a_B^2 + 2P_B a_B + Q_B \quad (9)$$

($b > 0$ for low field bifurcation and $b < 0$ for high field bifurcation). The potential for this slow coordinate is

$$U = \mp\tilde{\eta}s + \frac{b}{3}s^3, \quad (10)$$

while the distance between the saddle and the attractor is $\sqrt{\tilde{\eta}/|b|}$, thus the potential barrier for the slow coordinate is

$$\Delta U = \frac{4\tilde{\eta}^{3/2}}{3|b|^{1/2}(\Omega)}. \quad (11)$$

This is the well known $\xi = 3/2$ scaling law. A 1-dimensional FPE for $s$ can be written, a stationary solution for $\rho(s,\tilde{\eta},\Omega)$ obtained, and the escape rate calculated. This quantity will have the form $W = W'(\Omega)\exp(-\Delta U/D)$. Such adiabatic approach is valid only sufficiently close to the bifurcation point. When $\Omega \ll 1$, "sufficiently close" means that $\tilde{\eta} \ll \Omega^{-3}$. In this regime,

$$R \approx \begin{cases} \frac{4\sqrt{2}}{3}\Omega^{-1/2}\tilde{\eta}^{3/2} & \text{low field bifurcation} \\ \frac{4}{3^{1/4}}\Omega^{-1}\tilde{\eta}^{3/2} & \text{high field bifurcation} \end{cases} \quad (12)$$

A more systematic treatment of the close-to-a-bifurcation regime which will allow us to extract corrections to the adiabatic limit and derive the $\tilde{\eta} \ll \Omega^{-3}$ criterion will be considered in Section III.A

### 2. Low dissipation regime.

When effective friction, $\Omega^{-1}$ is low, the dynamics of $\vec{K}$ is approximately Hamiltonian: the time scale for the decay of energy is much larger then the time scale to make one cycle on the contour of approximately fixed energy. This separation of time scales breaks down very close to a bifurcation point, so as long as $\Omega^{-1} \neq 0$, there will always be a small fraction of the hysteresis displaying a $\xi = 3/2$ scaling. Aside from this very narrow region, the separation of time scales allows one to turn a 2-variable FPE into a 1-variable FPE for the diffusion of *energy*, by averaging out the fast part of the dynamics. The noise strength $D$ is proportional to $\Omega^{-2}$, so the FPE in the stationary regime can be rewritten as $\{g, \rho\} = -\Omega^{-1}\vec{\nabla} \cdot \left(\vec{r}\rho + D'\Omega^{-1}\vec{\nabla}\rho\right)$. Note that when $\Omega^{-1} = 0$, *any* function of the form $\rho(g(Q,P))$ will be a solution to this FPE. Therefore, we can expand $\rho(Q,P) = \rho^{(0)}(g(Q,P)) + \Omega^{-1}\rho^{(1)}(Q,P) + O(\Omega^{-2})$ and integrate over a contour of constant $g(Q,P)$. We will refer to such theory as "quasi-Hamiltonian" theory. After some algebra, this leads to:

$$\frac{d}{dE}\left(B(E)\rho^{(0)}(E) + D'\Omega^{-1}D(E)\frac{d\rho^{(0)}}{dE}\right) = 0 \qquad (13)$$

where $B(E) = \int\int_{g(Q,P)=E} dQ\, dP$ and $D(E) = \int\int_{g(Q,P)=E} \nabla^2 g(Q,P)\, dQ\, dP$. An alternative approach followed by [27] is to calculate an average rate of energy decay due to friction and an effective diffusion coefficient for the energy drift due to noise. These would turn out to be precisely the $B(E)$ and $D(E)$ respectively, hence Eq. (13) is the FPE for the energy. Returning back from $D'$ to $D$, the activation rate is $W \propto \exp(-R/D)$ where

$$R = -\Omega^{-1}\int_{E_a}^{E_s} \frac{B(E')}{D(E')}\, dE' \qquad (14)$$

Here $E_a$ is the energy of the attractor, and $E_s$ is the energy of the saddle. Close to bifurcation points, but not close enough for the overdamped theory to be applicable,

$$R \approx \begin{cases} 2\Omega^{-1}\tilde{\eta} & \text{low field bifurcation [18]} \\ \frac{4}{3^{1/4}}\Omega^{-1}\tilde{\eta}^{3/2} & \text{high field bifurcation [24]} \end{cases} \qquad (15)$$

Comparisson of Eqn. (15) with Eqn. (12) reveals that there must be a crossover from a $\xi = 1$ regime to $\xi = 3/2$ regime as $\sqrt{\beta}$ approaches $\sqrt{\beta_B^l}$.

## B. Power law scalings of escape barriers

When $\Omega^{-1} \neq 0$, sufficiently close to the saddle-node bifurcation, the dynamics near the attractor and the saddle is generically over-damped [29]. Hence, the soft-mode geometric picture offered in Section II.A.1 is generic and $\xi = 3/2$ is a genetic property in a system with finite damping and close enough to the saddle-node bifurcation. Further from the bifurcation, the over-damped soft mode does not exist. We have seen that for sufficiently low $\Omega^{-1}$, the overdamped $\xi = 3/2$ crosses over to $\xi = 1$ (close to $\sqrt{\beta_B^l}$) or remains $\xi = 3/2$ (close to $\sqrt{\beta_B^h}$). As recently proved by Dykman, Schwartz and Shapiro [27] (DSS), these are in fact also *generic* scaling laws in the under-damped vicinity of a saddle-node bifurcation. DSS considered two scenarios which may happen when $\Omega^{-1}$ *equals* zero. As $\tilde{\eta} \to 0$, the center and the saddle may merge, or they may remain separate. DSS named the first type of a *Hamiltonian* bifurcation "local" and the latter "non-local". The two situations dictate the form of the Hamiltonian $g$.

Let's switch to coordinates $(q,p)$ such that when $\Omega^{-1} = 0$, both the center and the saddle fixed points lie on the $p = 0$ axis. In the case of a local Hamiltonian bifurcation, in the vicinity of $(q = 0, p = 0, \tilde{\eta} = 0)$, $g$ is given by $g_L(q,p,\tilde{\eta}) = \frac{1}{2}p^2 + U_{cub}(q)$ where $U_{cub}(q) = -\frac{1}{3}q^3 + \tilde{\eta}q$. The center lies inside a small homoclinic loop at the energy of the saddle. DSS proved that given this form of the Hamiltonian $g$, addition of noise and damping leads to $R(\tilde{\eta}) = A(\Omega)\tilde{\eta}^{3/2}$ (in the under-damped regime). But we know that as as the system approaches the bifurcation even closer, it becomes over-damped, a soft-mode sets up and the method of analysis presented in Section II.A.1 leads to $R(\tilde{\eta}) = B(\Omega)\tilde{\eta}^{3/2}$. Therefore, assuming smooth dependence upon $\tilde{\eta}$, it must be that $A(\Omega) = B(\Omega)$. In other words, the $\xi = 3/2$ power law in this situation holds beyond where it was expected to hold due to a soft mode theory! In the Duffing system, a nonlocal bifurcation takes place at $\sqrt{\beta_B^h}$. In the numerical experiments described below, we found that the $\xi = 3/2$ power law holds near $\sqrt{\beta_B^h}$ over a *finite* range of $\tilde{\eta}$ even as $\Omega^{-1} \to 0$. This $\xi = 3/2$ law at zero $\Omega^{-1}$ has been predicted by [24], but the new work of DSS gives it a new explanation. We elaborate upon this in Section III.B.

In the case of a nonlocal Hamiltonian bifurcation, $g$ is given by $g_{NL}(q,p,\tilde{\eta}) = \frac{1}{2}p^2 + \tilde{\eta}U(q)$, where $U(q)$ is independent of $\tilde{\eta}$ and has a local minimum and maximum. The homoclinic loop of such systems has the property that only its size in the $p$-direction shrinks to zero as $\tilde{\eta} \to 0$, while the distance between the center and the saddle inside the loop remains finite. Introduction of damping into these types of systems will not change the separation between the saddle and the attractor until the system has come close enough to the bifurcation: $\tilde{\eta} \sim \Omega^{-2}$. DSS proved that given this form of the Hamiltonian $g$, addition of noise and damping leads $R(\tilde{\eta}) \propto \tilde{\eta}$ (in the underdamped regime). Therefore, at finite $\Omega^{-1}$ we expect a $\xi = 1$ scaling moderately close to the bifurcation, but further away then the region of over-damped $\xi = 3/2$ scaling. In the Duffing system, a nonlocal bifurcation takes place at $\sqrt{\beta_B^l}$. It is important to stress that

all saddle-node bifurcations at *finite* $\Omega^{-1}$ are local in the sense that the attractor and the saddle merge as $\tilde{\eta} \to 0$. The terms "local" or "nonlocal" only make sense at zero $\Omega^{-1}$. We must also mention that a nonlocal bifurcations may take place in many forms. For example, in a Duffing oscillator, the homoclinic loop has a horse-shoe shape at $\Omega^{-1} = 0$ which becomes thinner while remaining extended as $\tilde{\eta} \to 0$. DSS found a change of variables which maps from $g$ to $g_{NL}$.

## III. NUMERICAL METHOD AND RESULTS

Numerical calculations of escape rate are based on direct evaluation of $S^*$. The algorithm for doing so is as follows. (1) Choose parameters $\Omega^{-1}$ and $\sqrt{\beta}$. (2) Calculate repulsive eigenvectors (i.e. those whose eigenvalues have positive real part) of the FP $(Q_{attr}, P_{attr}, p_Q = 0, p_P = 0)$ of the auxiliary system. These eigenvectors span the tangent plane to the unstable manifold of this attractor. (3) Position a locus of initial conditions on a small circle that lies on this tangent plane and centered around this FP and evolve each of these initial conditions according Hamiltonian equations with Hamiltonian $\mathcal{H}$ from Eqn. (4). The angle around this circle, $\varphi$, serves as a parameter that enumerates a trajectory. (4) From this set of trajectories, find the one which leads into the saddle, with a special trajectory parameter $\varphi^*$. Because the method involves "shooting" many trajectories to see which one hits the saddle, this method is occasionally called "the shooting method". (5) Evaluate the action along this trajectory. For each $\Omega^{-1}$, this procedure would be repeated for many values of $\sqrt{\beta}$ between $\sqrt{\beta_B^l}$ and $\sqrt{\beta_B^h}$.

In practice, step (4) may require several rounds of bracketing. In each round, for each trajectory, we calculate the distance between the saddle and the point of intersection of that trajectory with the separatrix, measured along the separatrix. We identify a $\varphi$ for which the trajectory came closest to the saddle and then evolve another set of trajectories in a small range of trajectory parameters around this $\varphi$. After more and more rounds of such procedure, we would obtain a trajectory that hits the separatrix closer and closer to the saddle. In general, finding a trajectory that connects an attractor with the saddle is difficult because it lies on the intersection of the unstable manifold of the attractor and the stable manifold of the saddle in the 4D auxiliary space [22], [32]. A small deviation of $\varphi$ on opposite side of $\varphi^*$ will produce trajectories that lie on opposite sides of this intersection and will diverge from each other. This effect is most pronounced closer to bifurcations because the motion along the optimal trajectory becomes much slower then the diverging motion away from it - such is the structure of eigenvalues of both attractor and saddle close to the bifurcation. This polarity takes place only close to bifurcation points, but it persists further away from bifurcation points when $\Omega^{-1}$ is larger. Therefore, in the small-$\Omega^{-1}$ regime, finding a trajectory between an attractor and the saddle is difficult only very close to bifurcation points, but in the large-$\Omega^{-1}$ regime, finding such a trajectory is difficult over a larger part of the hysteresis.

We will now summarize results of the computation of $S^*$, scaling laws, and crossovers. It is sometimes easier to present results in terms of $x = \frac{\tilde{\eta}}{\sqrt{\beta_B^r} - \sqrt{\beta_B^l}}$ - "reduced" $\tilde{\eta}$. For each $\Omega^{-1}$ and each type of transition, we scanned the hysteretic region at multiple values of $x$ and for each $x$ we followed the "shooting" procedure, and where necessary, the bracketing method.

### A. Up → Down transitions

#### 1. Numerical results

A plot of $S^*/\Omega^{-1}$ versus $x$, Figs. 4, 8 reveals several features. At low $\Omega^{-1}$ two regimes clearly stand out: one with $\xi \approx 3/2$, and one with $\xi \approx 1$. Further from the bifurcation, the $\xi = 1$ scaling law breaks down and $S^*/\Omega^{-1}$ versus $x$ displays a non-power-law behavior. For various values of $\Omega^{-1}$, the data in the "3/2 regime" fits well to

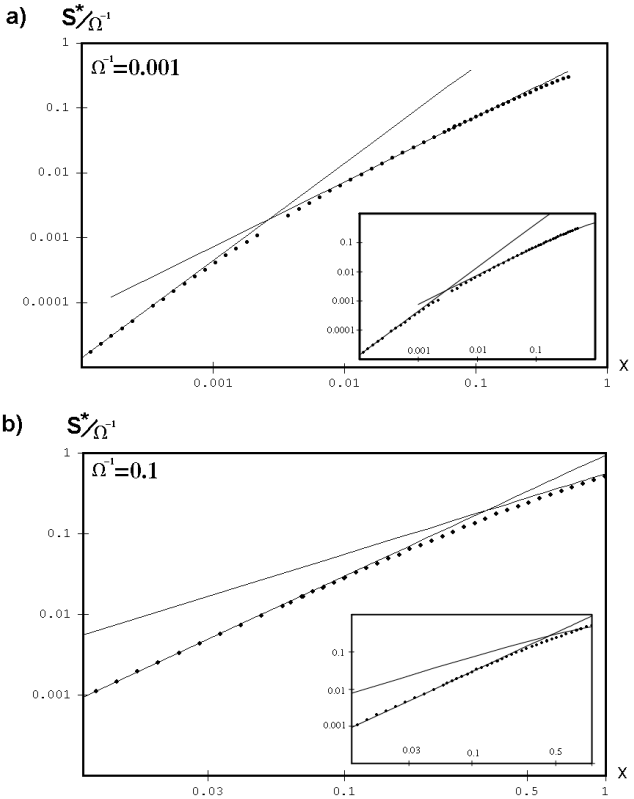


FIG. 4: Main plots: $S^*(x)/\Omega^{-1}$ (dots) and *fits* (lines) for up → down transitions. The fit to the $\xi = 3/2$ regime was made by analyzing $\ln\left(S^*/\Omega^{-1}\right)$ vs. $\ln x$ and a fit to the $\xi = 1$ regime was made by analyzing $S^*/\Omega^{-1}$ vs. $x$. Inserts: $S^*(x)/\Omega^{-1}$ (dots) and *theory* (lines) based on Eqn. 12 for the $\xi = 3/2$ regime and Eqn. 15 for the $\xi = 1$ regime.

a power law with $\xi$ which is up to 3% below the theoretical value of 3/2. In general, *precise* extraction of the exponent 3/2 requires approaching very close to the bifurcation. It appears that the discrepancy was highest in those cases when the bifurcation was approached less closely (relative to the crossover point) or less reliably. The reliability of the approach is hampered at larger $\Omega^{-1}$ by the strong divergence of trajectories explained in the previous section. A crossover between the $\xi = 3/2$ and $\xi = 1$ regime is defined to be such $x$ at which fits to the respective regions intersect. Collecting data for $S^*$ vs. $x$ for various $\Omega^{-1}$ we were able to map out the entire bi-stability region for locations of various scaling regimes and crossovers between them. The lowest $\Omega^{-1}$ at which computations were made was $10^{-3}$. The product of this work is depicted in Fig. 5. It is important to stress that in Fig. 5 for up $\rightarrow$ down transitions and in Fig. 9 for down $\rightarrow$ up transitions, the mapping was performed by scanning $\sqrt{\beta}$ while holding $\Omega^{-1}$ fixed.

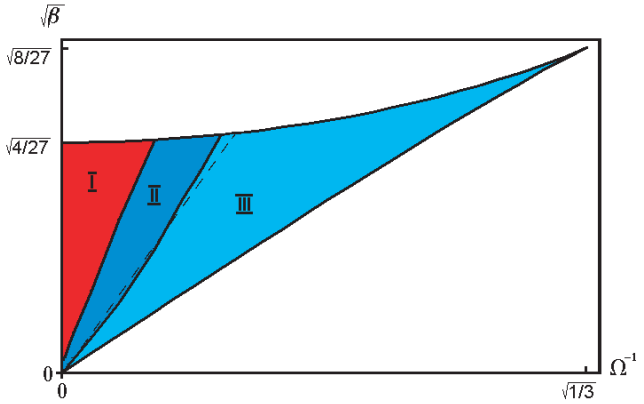


FIG. 5: Regions of different scaling behaviors for up $\rightarrow$ down transitions obtained by scanning $\sqrt{\beta}$ at fixed $\Omega^{-1}$ at multiple values of $\Omega^{-1}$. Region I - non-power-law regime. Region II - $\xi = 1$ regime and region III - $\xi = 3/2$ regime. The crossover between the $\xi = 1$ and a non-power law regime was defined as the point at which the fit to $\xi = 1$ regime came closest to the $\ln\left(Q^*/\Omega^{-1}\right)$ vs. $\ln x$ - see Fig. 4.

Note that as $\Omega^{-1} \rightarrow 0$, the linear scaling is found between $x = 0$ and some finite $x$. At small, but non-zero $\Omega^{-1}$, the region of $\xi = 3/2$ subsequently grows. These results are in accord with the theorem of DSS which states that close to a bifurcation which at $\Omega^{-1} = 0$ becomes nonlocal, in the underdamped regime at non-zero $\Omega^{-1}$ the $\xi$ is expected to be 1. Since the underdamped portion of the hysteresis extends all the way to the bifurcation as $\Omega^{-1} \rightarrow 0$, we expect the linear scaling to extend all the way to the bifurcation in this limit [33].

Clearly, the boundaries between regions I, II and III are purely conventional - they have been defined in some convenient way, but do not correspond to anything specifically physical. To emphasize this point, it helps to construct a 3-dimensional plot of $S^*/\Omega^{-1}$ versus $x$ and $\Omega^{-1}$ - Fig. 6. This surface is smooth and large parts of it

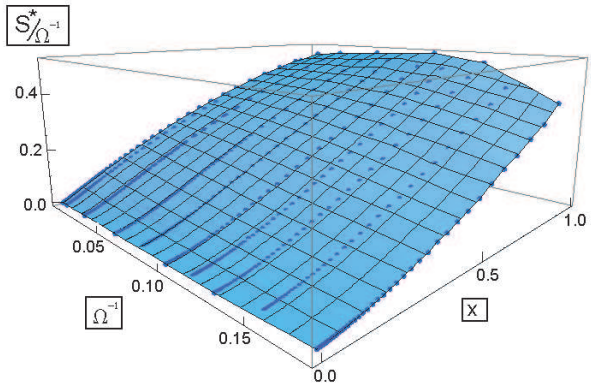


FIG. 6: $S^*/\Omega^{-1}$ versus $x$ and $\Omega^{-1}$ up to $\Omega^{-1} = 0.175$ which is about 30% of the hysteresis. Fig. 4 are two slices of this surface.

happen to fit well to power laws. The regions when this is possible appear to be much bigger then the regions at which the $\xi = 1$ and $\xi = 3/2$ scaling was supposed to be applicable on the basis of approximations discussed in Section II. A natural question is why this is so! To shed more light on this issue, let's digress on the crossover from the $\xi = 3/2$ to $\xi = 1$ in more detail.

### 2. *Discussion of the $\xi = 3/2$ to $\xi = 1$ crossover*

Notice that the crossover between the $\xi = 3/2$ and $\xi = 1$ regime, as it appears in Fig. 4 was defined as the point of intersection of the fits to the respective regimes. Thus, to predict this crossover we simply equate the asymptotic in the $\xi = 3/2$ regime, $R = \frac{4\sqrt{2}}{3}\Omega^{-1/2}\tilde{\eta}^{3/2}$ to the asymptotic in the $\xi = 1$ regime $R = 2\Omega^{-1}\tilde{\eta}$ (this is most accurate as $\Omega^{-1} \rightarrow 0$). The result is $\tilde{\eta} = \frac{9}{8}\Omega^{-1}$, which corresponds to $\sqrt{\beta} = \sqrt{\beta_B^l} + \frac{9}{8}\Omega^{-1}$ $\left(\sqrt{\beta_B^l}\text{is itself a function of } \Omega^{-1}\right)$. The cross-over predicted this way is depicted by dashed line in Fig. 5. The fact that this method of predicting a crossover works well tells us that the asymptotic expressions are correct. However, we could imagine that the width of the crossover region was very large, in which case the crossover defined by equating the fits and predicted by equating the asymptotics is not physically meaningful. The width of the crossover region is a more physically interesting quantity. Alternatively we may also define the following two crossovers: a "lower crossover" (LC) defined as a characteristic value of $\sqrt{\beta}$ (or $\tilde{\eta}$ or $x$) above which the $\xi = 3/2$ regime begins to fail and an "upper crossover" (UC) defined as a characteristic value of $\sqrt{\beta}$ (or $\tilde{\eta}$ or $x$) below which the $\xi = 1$ regime begins to fail. The width of the crossover region is the difference between these two values.

Physically, we expect the LC to take place where the soft-mode picture fails. Therefore, a good *characteristic* estimate of this will be such $\tilde{\eta}$ at which the real and imaginary parts of eigenvalues become equal. This can be shown to happen for $\tilde{\eta} = \Omega^{-3}/2$ - the scaling is *cubic*.

To predict the LC more accurately let's turn back to the type of analysis described in section II.A.1. Let's re-write Eqns. (5)-(6) for the non-adiabatic part of the fast variable, $A = f - a_B s$. Near low-field bifurcation, these will have the form

$$\dot{A} = -a_B\tilde{\eta} - 2\Omega^{-1}A + a_1 s^2 + a_2 As + a_3 A^2 + a_4 s^3 + a_5 s^2 A + a_6 sA^2 + a_7 A^3 + n_x - a_B n_y \quad (16)$$

$$\dot{s} = \tilde{\eta} + b_1 s^2 + b_2 As + b_3 A^2 + b_4 s^3 + b_5 As^2 + b_6 A^2 s + b_7 A^3 + n_y \quad (17)$$

All coefficients $a_i$ and $b_i$ are functions of $\Omega^{-1}$. The position of fixed points sets the characteristic scaling of $A$ to be $\tilde{\eta}$ and of $s$ to be $\tilde{\eta}^{1/2}$ (generic feature of saddle-node bifurcations), so we define new variables: $s = \tilde{\eta}^{1/2}s'$ and $A = \tilde{\eta}A'$. Moreover, the $\Omega$-dependencies of the coefficients $a_i$ and $b_i$ near low-field bifurcation are such that when $\Omega^{-1}$ is small compared to 1, further re-scaling of $s'$ and $A'$ as $s' = \Omega^{-1/2}\sigma$ and $A' = \Omega^2\phi$ yields a single dimensionless parameter $\mu = \tilde{\eta}\Omega^3$; such reduction is approximate, but becomes more accurate for smaller $\Omega^{-1}$ [34]. In terms of $\mu$, $\sigma$ and $\phi$ we have

$$\frac{d\phi}{d\tau} = \left(-1 - 2\phi + \frac{3}{2}\sigma^2\right) + \mu^{1/2}\left(\sigma\phi + \sigma^3\right) + \mu\left(3\phi\sigma^2 - \frac{\phi^2}{2}\right) + \mu^{3/2}3\sigma\phi^2 + \mu^2\phi^3 + N_\phi \quad (18)$$

$$\frac{d\sigma}{d\tau} = \mu^{1/2}\left(1 - \frac{\sigma^2}{2}\right) + \mu\left(\sigma\phi - \sigma^3\right) + \mu^{3/2}\left(\frac{3}{2}\phi^2 - 3\sigma^2\phi\right) - \mu^2 3\sigma\phi^2 - \mu^{5/2}\phi^3 + N_\sigma \quad (19)$$

where $\tau = \Omega^{-1}T$. With the help of the definition of $\sigma$ and Eq. (7) we note that the zeroth-order part of the fast variable $a_B s$ is given by $\tilde{\eta}^{1/2}\Omega^{1/2}\sigma$ and the correction due to non-adiabaticity of the fast variable is $A = \tilde{\eta}\Omega^2\phi$. We also see from Eqs. (18)-(19) that when $\mu \ll 1$, both $\sigma$ and $\phi$ are $O(1)$. Hence comparison of the two terms says that when $\mu \ll 1$, *non-adiabatic part/adiabatic part* $\sim (\tilde{\eta}\Omega^2)/(\tilde{\eta}^{1/2}\Omega^{1/2}) = \mu^{1/2} \to 0$ as $\mu \to 0$. In other words, in this regime the non-adiabatic part becomes unimportant and the problem reduces to 1 dimension defined by the noisy dynamics of the slow variable. To do this reduction explicitly, we first notice from Eqs. (18)-(19) that at lowest order, the variable $\sigma$ can be considered constant while $\phi(\sigma) \approx \frac{3}{4}\sigma^2 - \frac{1}{2}$ + non-adiabatic corrections. This $\phi(\sigma)$ is then substituted into Eq. (19). The resulting expression can only be considered up to $O(\mu)$ since the higher-order terms must also include the non-adiabatic corrections to $\phi$ to be complete [note that if the $\mu^{1/2}$-terms in Eq. (19) contained any $\phi$ terms, the complete expression within the adiabatic approximation would only extend to $O(\mu^{1/2})$, not $O(\mu)$]. The barrier height in the resultant 1-dimensional potential is $\Delta U = \frac{4\sqrt{2}}{3}\mu^{1/2} + \sqrt{2}\mu^{3/2}$. Again, the correction is within the adiabatic approximation; a non-adiabatic correction would be higher order in $\mu$. Taking into account that the $N_\sigma$ has a diffusion constant $D_\sigma = \frac{\Omega^2}{\tilde{\eta}}D$, we have

$$R = \frac{4\sqrt{2}}{3}\Omega^{-1/2}\tilde{\eta}^{3/2} + \sqrt{2}\Omega^{5/2}\tilde{\eta}^{5/2} \quad (20)$$

[compare with Eq. (12)]. We see again that the correction term grows to be dominant when $\mu \sim 1$ (i.e. when $\tilde{\eta} \sim \Omega^{-3}$) , but this is precisely when the non-adiabatic part becomes comparable to the adiabatic part, and it turns out to be meaningless to treat the problem as effectively 1-dimensional. Our analysis taught us that in the regime when $\tilde{\eta} \ll \Omega^{-3}$, the activation barrier $R$ will scale as $\tilde{\eta}^{3/2}$ to a good approximation. Outside the regime of $\tilde{\eta} \ll \Omega^{-3}$ the current analysis only allows us to conclude that if $\xi$ remains to be 3/2, the physics behind this scaling is not a physics of a 1-dimensional over-damped soft mode; the escape problem is not 1-dimensional for $\tilde{\eta} \gg \Omega^{-3}$.

To answer the question of what happens outside of the $\tilde{\eta} \gg \Omega^{-3}$ regime we chose to compute the most likely escape path numerically and calculate $S^*$ on that path. We looked at the difference between the zeroth-order theory, $R_0 = \frac{4\sqrt{2}}{3}\Omega^{-1/2}\tilde{\eta}^{3/2}$ and the numerically-computed $S^*$. This was repeated for several values of $\Omega$ and in each case, a fit to the function $\propto \tilde{\eta}^p$ was made. Although this represents computer calculations, the data is somewhat noisy due to the difficulty of hitting the saddle. Values of $p$ between 2.15 and 2.86 were found. The predicted

value of $p = 5/2$ in the correction factor lies in the middle of this range. However, the crossover LC, defined as an intersection of some small fraction $r$ of $R_0$ with a fit to $R_1$ scales *linearly* with $\Omega^{-1}$, not cubically. The $\tilde{\eta}_{LC}$ so obtained can be fit to a power law with exponent 1.2 for $r = 0.1$ and and 1.1 for $r = 0.2$ - both of these exponents are far from 3.

The question of why the $\xi = 3/2$ scaling holds over a much larger region of parameter space then expected based on the 1-dimensional soft-mode picture remains unanswered, and forms a good challenge problem for a future work. One potential hypothesis is that in the region when the 1-dimensional soft-mode picture does not hold true, the action along the MPEP actually grows only over a small portion of the MPEP where the motion is essentially 1-dimensional. We provide plot of the action versus the distance along the trajectory, $S(\ell)$ and the derivative $dS/d\ell$ for a particular value of parameters deep in region III - Fig. 7. The derivative plot clearly shows that action grows fastest in the last winding of the trajectory, but this is not sufficient to conclude that the dynamics in that part of the trajectory can somehow be described as effectively 1-dimensional.

Similarly to the LC, the UC can be defined as a characteristic value of the driving field *below* which the linear scaling begins to break down. To predict this point, we must again compare the lowest and one higher order terms in the theory for $R(\tilde{\eta})$ that applies in the $\xi = 1$ regime. The effect of a non-zero $\Omega^{-1}$ is clearly seen in Fig. 8 The lowest-order in dissipation theory (quasi-Hamiltonian) indeed predicts linear scaling for low values of $\tilde{\eta}$ (or $x$), which according to Eq. (15) is given by $2\Omega^{-1}\tilde{\eta}$. The region of linear scaling persists for non-zero $\Omega^{-1}$, but due to the existence of the 3/2-scaling region, this linear part has been "pushed over" to larger $\tilde{\eta}$ and to lower values then those predicted by the zeroth-order theory. A work by Chinarov' et. al. [25] worked out dissipative corrections to the quasi-Hamiltonian theory to next order in $\Omega^{-1}$. Translating their results to our notation reads: $R = \Omega^{-1}\left(2\tilde{\eta} - \pi\Omega^{-1}\right)$ (compare with Eq. 15). The factor $\pi\Omega^{-2}$ is just that correction which takes this lowering into account. We expect the linear scaling to start breaking down when the correction reaches some fraction $r$ of the zeroth-order term, i.e. when $\tilde{\eta}_{UC} = \frac{\pi}{2r}\Omega^{-1} \approx \frac{\pi}{2r}\Omega^{-1}$ for low $\Omega^{-1}$. To extract $\tilde{\eta}_{UC}$ from the data we subtracted the zeroth-order part from $S^*/\Omega^{-1}$. The resulting function grows for low $\tilde{\eta}$, slows down for intermediate $\tilde{\eta}$ (but not completely because the exact slope in the linear regime is slightly different from the zeroth-order result) and increases for yet larger $\tilde{\eta}$ past the linear regime (see Fig. 6). The average value in the intermediate regime is taken to be the offset factor. Equating this correction to the zeroth order term yields $\tilde{\eta}_{UC}$ which does depend linearly on $\Omega^{-1}$.

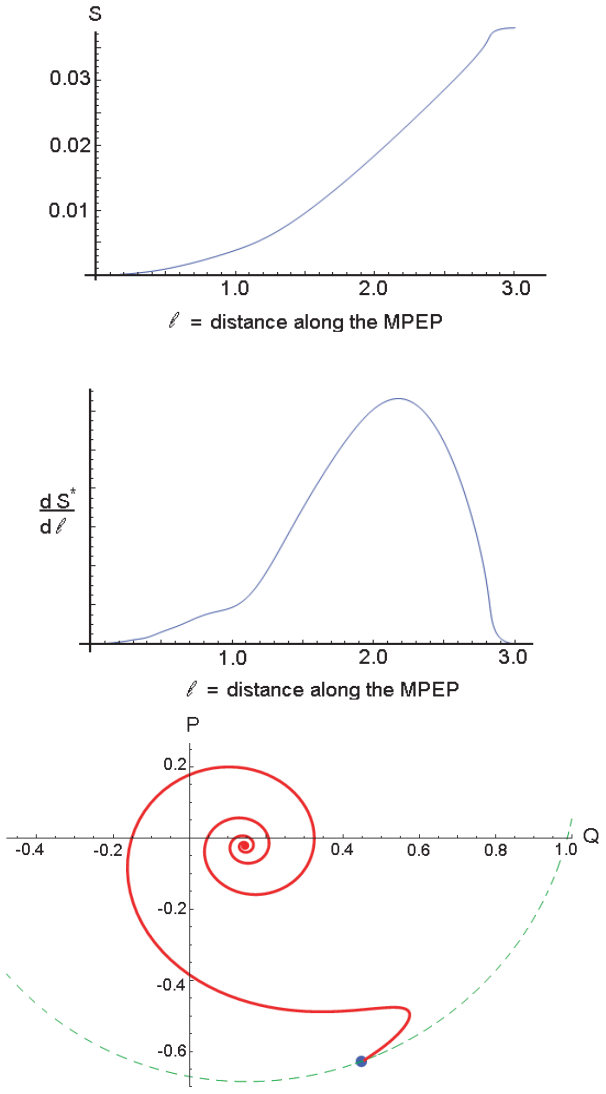


FIG. 7: $S(l)$ and its derivative for particular parameters in region III as well as the plot of the MPEP (dashed curve denotes separatrix). Here $\Omega^{-1} = 0.15$ and $\sqrt{\beta} = 10\%$ of the hysteresis. These parameters correspond to $\mu \approx 5$; the soft-mode picture is expected to hold only for $\mu \ll 1$.

### B. Down → Up transitions

Analogously to the up → down transitions, the entire bi-stability region was mapped out. The product of this mapping is shown in Fig. 9. The lowest $\Omega^{-1}$ at which computations were made was 0.005. Fuzzy regions correspond to those sections of the $\sqrt{\beta}$ - $\Omega^{-1}$ plane which proved exceptionally difficult to map reliably due to high divergence of trajectories. A portion of the surface $S^*/\Omega^{-1}(x, \Omega^{-1})$ is presented in Fig. 10.

The low amplitude basin does not exhibit nonlocal geometry upon approach to the bifurcation at zero $\Omega^{-1}$, and correspondingly, the linear scaling is not found in down → up transitions at any $\Omega^{-1}$ (see Fig. 11), which

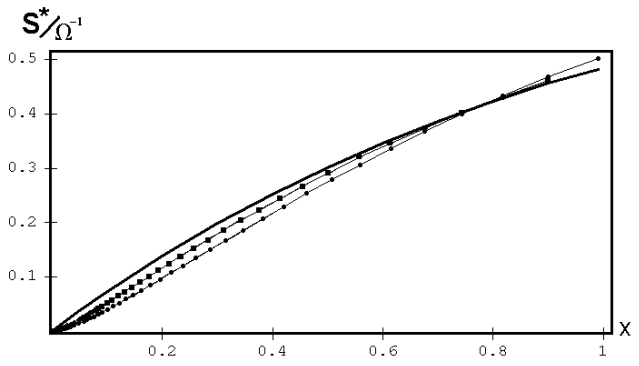


FIG. 8: $R^*(x)/\Omega^{-1}$ on a linear scale. The thick black line represents the zeroth-order theory, Eq. (14). The other curves represent numerical calculations of $S^*$ - squares: $\Omega^{-1} = 0.03$, circles: $\Omega^{-1} = 0.06$.

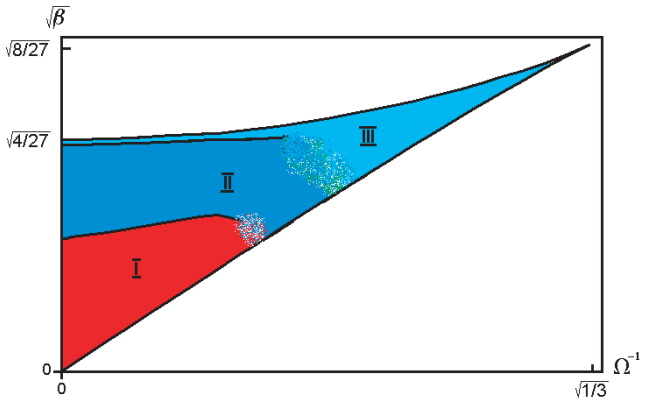


FIG. 9: Regions of different scaling behaviors for down → up transitions obtained by scanning $\sqrt{\beta}$ at fixed $\Omega^{-1}$ at multiple values of $\Omega^{-1}$. Region I corresponds to a non-power-law regime. Region II corresponds to the $\xi \approx 1.3$ regime. Region III corresponds to the $\xi = 3/2$ regime.

is in accord with the DSS theorem. The $\xi = 3/2$ scaling gives way to a different scaling relationship further from the bifurcation, with an exponent $\xi \approx 1.3$. We interpret this $\xi \approx 1.3$ exponent as a power-law interpolation.

Note that region III in Fig. 9 (the $\xi = 3/2$ region) extends all the way to zero $\Omega^{-1}$ - this is unlike section II, where the $\xi = 3/2$ region disappears as $\Omega^{-1} \to 0$. These results are in accord with the theorem of DSS which states that close to a bifurcation which is local at $\Omega^{-1} = 0$, in the underdamped regime at non-zero $\Omega^{-1}$ the $\xi$ is expected to be 3/2. Since the underdamped portion of the hysteresis extends all the way to the bifurcation as $\Omega^{-1} \to 0$, we expect the 3/2 scaling to extend all the way to the bifurcation in this limit. Had we assumed that $\xi = 3/2$ due to the over-damped soft mode, we would follow the nearly-adiabatic analysis of the previous section and we would find that for low $\Omega^{-1}$ there exists another dimensionless parameter $\nu = \tilde{\eta}^{1/2}\Omega^2$ [35].

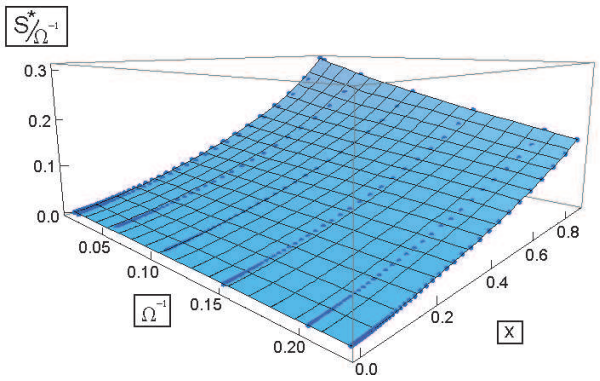


FIG. 10: $S^*/\Omega^{-1}$ versus $x$ and $\Omega^{-1}$ up to $\Omega^{-1} = 0.22$ which is about 33% of the hysteresis. Fig. 4 are two slices of this surface.

When $\nu \ll 1$ such analysis predicts that $\xi = 3/2$. When $\nu \sim 1$, the reduction to 1-d due to adiabaticity becomes impossible and prediction based on this method can not be made. The fact that $\xi$ remains 3/2 beyond $\nu \ll 1$, as we see from numerics, indicates that the 3/2 scaling is not a consequence of reduction to an over-damped 1-d soft-mode.

In the previous section we offered three definitions of the $3/2 \to 1$ crossover. In the case of up → down transitions, we don't have theory for the $\xi \approx 1.3$ scaling regime, so the crossover from the 3/2 scaling can be defined here only as a point at which the 3/2 scaling begins to break. Since the 3/2 scaling is predicted by the quasi-Hamiltonian theory, we look at next order corrections due to Chinarov et. al [25]. Translating the results of that work to our notation, close to the bifurcation, $R \approx \frac{4}{3^{1/4}}\Omega^{-1}\tilde{\eta}^{3/2} + 1.06\frac{4}{3^{1/4}}\Omega^{-3}\left|\ln\Omega^{-1}\right|\tilde{\eta}^{3/2}$ (compare with Eq. 15). Evidently, the correction is to simply shift $R(\tilde{\eta})$ by a constant offset (see Fig. 11 (b) where this effect is clearly pronounced throughout the entire $R(\tilde{\eta})$, not just close to the bifurcation). Because the correction is so small for small $\Omega^{-1}$, its effect doesn't become noticeable until a rather large $\Omega^{-1}$ - equating the zeroth-order term to the correction term predicts this value of $\Omega^{-1}$ to be $\approx 1.5$. Qualitatively, this delayed effect is observed in numerics (see Fig. 9), but the crossover doesn't seem to depend on $\Omega^{-1}$ significantly until $\Omega^{-1} \approx \Omega_c^{-1}/2 \approx 0.28$.

## IV. CONCLUSION

We considered the escape rate $W \propto \exp(-R/D)$ from one basin of a non-linear oscillator into another. We calculated the leading term in the effective barrier $R$ in the limit of small noise: $\ln W = -R(\Omega^{-1}, \sqrt{\beta})/D + O(D^0)$. For any given $\Omega^{-1}$, this $R$ may exhibit several scaling behaviors versus $\left|\sqrt{\beta} - \sqrt{\beta_B}\right|$ where $\sqrt{\beta_B}$ is a value of the driving field at which a saddle-node bifurcation takes place. We used numerical shooting method to calculate

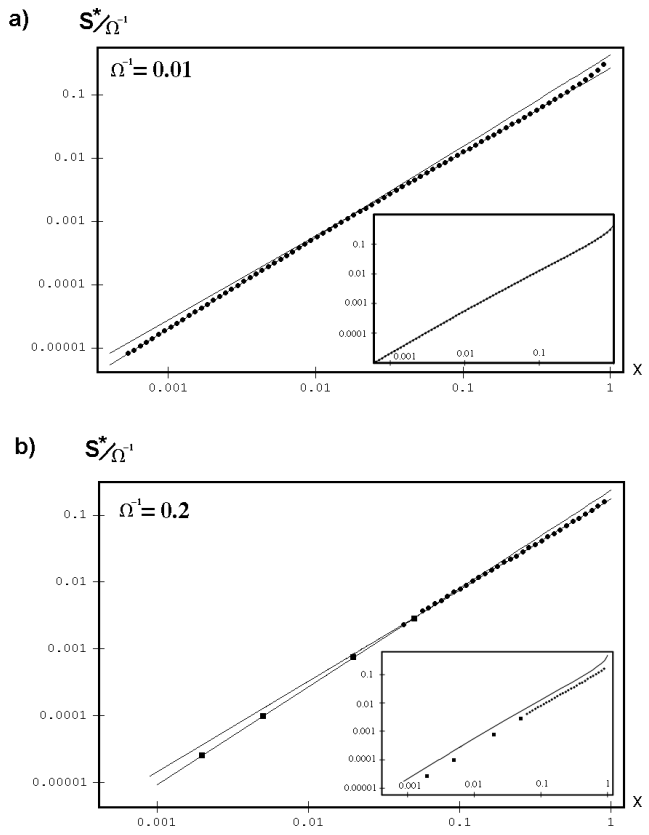


FIG. 11: Main plots: $S^*(x)/\Omega^{-1}$ (dots) and *fits* (lines) for down $\rightarrow$ up transitions. Fits to the $\xi = 3/2$ and $\xi \approx 1.3$ regimes was made by analyzing $\ln\left(S^*/\Omega^{-1}\right)$ vs. $\ln x$. The region where the simple shooting method was unreliable for hitting the saddle (due to high divergence of trajectories), a bracketing method was used, the results of which are denoted by squares. Inserts: $S^*(x)/\Omega^{-1}$ (dots) and *theory* (lines) based on Eqn. 14 for the $\xi = 1$ regime; note that this quasi-Hamiltonian theory predicts the $\xi = 3/2$ scaling, as was first pointed out by [24] and in light of the recent work by [27] this fact has been explained to be a result of the fact that this bifurcation is local at $\Omega^{-1} = 0$.

most probable escape paths (MPEPs) from one basin to another. $R$ is the action along this MPEP between an attractor inside one of the basins and the saddle that lies on the separatrix between the two basins. This technique allowed us to map out the $\sqrt{\beta}$ - $\Omega^{-1}$) parameter space for locations of various scaling behaviors of $R$ versus $\left|\sqrt{\beta} - \sqrt{\beta_B}\right|$. The result of this mapping is shown in Fig. 5 for up $\rightarrow$ down transitions and in Fig. 9 for down $\rightarrow$ up transitions.

We confirmed predictions of the recent work by Dykman, Schwartz and Shairo (DSS) [27], which classifies scaling laws based on the structure of the homoclinic trajectory at the energy of the saddle zero $\Omega^{-1} = 0$ - "local" or "nonlocal". We found that for those bifurcations which become nonlocal when $\Omega^{-1} = 0$, at non-zero $\Omega^{-1}0$ there exists a regime with $R \propto \left|\sqrt{\beta} - \sqrt{\beta_B}\right|$, as predicted by DSS. Such situation occurs for up $\rightarrow$ down transitions close to the low-field bifurcation. Even closer to the low-field amplitude bifurcation we found a crossover into the $R \propto \left|\sqrt{\beta} - \sqrt{\beta_B}\right|^{3/2}$ regime. We have defined this crossover in three different ways. Following one of the definitions we discovered that the 3/2-scaling breaks down much further from the bifurcation then where it would be expected to break down if the physics of this scaling was due to an over-damped soft mode.

We also found that for those bifurcations which are local when $\Omega^{-1} = 0$, at non-zero $\Omega^{-1}$ there exists a regime with $R \propto \left|\sqrt{\beta} - \sqrt{\beta_B}\right|^{3/2}$, which holds over a finite potion of a hysteresis even as $\Omega^{-1} \rightarrow 0$. Such situations take place for down $\rightarrow$ up transitions close to the high-field bifurcation (this has been predicted earlier [24]). This 3/2 scaling again takes place much further from the bifurcation then were it would be expected to hold as a result of over-damped soft mode, but for the down $\rightarrow$ up transitions this fact is somewhat less novel because it has been explicitly predicted to hold in the limit of $\Omega^{-1} \rightarrow 0$ a long time ago by [24] and also by recent work of DSS as explained in Section II.B. Further from the high-field bifurcation, we found another crossover into a regime $R \propto \left|\sqrt{\beta} - \sqrt{\beta_B}\right|^{\xi}$ where $\xi \approx 1.3$. A crossover into power law regime was not expected on any analytical grounds, so we interpret this power law as an interpolation.

The author expresses deep gratitude to Mark Dykman for his guidance on this project. A short publication with Dr. Dykman will appear elsewhere. The author also thanks Michael Cross for numerous useful discussions and acknowledges the support from the NSF Grant No. DMR-0314069.

[1] Kramers, Physica **VII, 4**, 284 (1940).
[2] J. Kurkijarvi, Phys. Rev. B **6**, 832 (1972).
[3] R. H. Victora, Phys. Rev. Lett. **63**, 457 (1989).
[4] M.I. Dykman, M.A. Krivoglaz, Physica **104A**, 480-494 (1980).
[5] O. A. Tretiakov, Phys. Rev. B **67**, 073303 (2003).
[6] K. A. Wiesenfeld and E. Knobloch, Phys. Rev. A **26**, 2946 (1982).
[7] R. S. Maier and D. L. Stein, Phys. Rev. Lett. **86**, 3942 (2001).
[8] D. Ryvkine, M. I. Dykman, and B. Golding, Phys. Rev. E, **69**, 061102 (2004).
[9] A.N. Cleland and M.L. Roukes, J. of App. Phys. **92**, 2758 (2002).
[10] J. S. Aldrige and A.N. Cleland, Phs. Rev. Lett. **94**, 156403 (2005).
[11] H. W. Ch. Postma, I. Kozinsky, A. Husain, M.L. Roukes, Appl. Phys. Lett. **86**, 223105 (2005).

[12] I. Kozinsky, H. W. Ch. Postma, O. Kogan, M. Roukes, Phys. Rev. Lett. **99**, 207201 (2007).

[13] C. A. Stambaugh and H. B. Chan, Phys. Rev. B, **73**, 172302 (2006).

[14] I. Siddiqi, et. al. Phys. Rev. Lett. **93**, 207002 (2004).

[15] K. Kim et. al. Phys. Rev. A 72, 053402 (2005).

[16] R. Almog, S. Zaitsev, O. Shtempluck, and E. Buks, Appl. Phys. Lett. **90**, 013508 (2007).

[17] B. Abdo, E. Segev, O. Shtempluck, and E. Buks, J. App. Phys. **101**, 083909 (2007).

[18] M.I. Dykman and M. A. Krivoglaz, Sov. Phys. JETP **50**, 30 (1979).

[19] R.P. Feynman, A.R. Hibbs, *Quantum mehcanics and path integrals*, (New York, McGraw-Hill, 1965).

[20] M.I. Freidlin, A.D. Wentzell, *Random perturbations of dynamical systems*, (New York, Springer, 1998).

[21] L.S. Schulman, *Techniques and Applications of Path Integration*, (Mineola, Dover, 2005).

[22] D. L. Stein, R. S. Maier, SIAM J. Appl. Math. 57, 752 (1997).

[23] J. D. Crawford, Rev. Mod. Phys. **63**, 991 (1991).

[24] A.P. Dmitriev, M.I. D'yakonov, Zh. Eksp. Teor. Fi. **90**, 1430-1439, (1986). Sov. Phys. JETP 63, 838 (1986).

[25] V. A. Chinarov, M.I. Dykman, V.N. Smelyanskiy, Phys. Rev. E **47**, 2448 (1993).

[26] M. I. Dykman, Phys. Rev. E **75**, 011101 (2007).

[27] M.I. Dykman, I.B. Schwartz, M. Shapiro, Phys. Rev. E **72** 021102 (2005).

[28] Such envelope dynamics is described in many sources, all using somewhat different notation. For example: A. H. Nayfeh and D. T. Mook, *Nonlinear oscillations* (John Wiley, New York, 1979); N.N. Bogoliubov and Y.A. Mitropolsky, *Asymptotic Methods in the Theory of Nonlinear Oscillations* (Gordon and Breach Science Publishers, New York, 1961). See also L. Landau and Y. Lifshitz, *Mechanics* (Addison-Wesley, Reading, MA 1960) for a terse discussion of nonlinear oscillations.

[29] J. Guckenheimer and P. Holmes, *Nonlinear Oscillators, Dynamical Systems and Bifurcations fo Vector Fields* (Springer-Verlag, NY 1987); V. Arnold, *Ordinary Differential Equations*, 3rd ed. (Springer, New York, 1992).

[30] Physics Letters A **195**, 53-58 (1994).

[31] Phys. Rev. E, **55**, 2369 (1996).

[32] The question of *existence* of this intersection, to our knowledge, is not a fully understood one.

[33] In practice we could go down to $\Omega^{-1} = 0.001$. In principle, strictly at $\Omega^{-1} = 0$ escape trajectories do not exist; they only have meaning in the limit $\Omega^{-1} \to 0$.

[34] From our definitions, $\omega_F = \omega_0 \left(1 + \frac{1}{Q\Omega^{-1}}\right)$. Recall that in order for equations (2)-(3) to apply, we must be working in the regime when $\omega_F = \omega_0(1 + \text{small number})$. Therefore, if the limit $\Omega^{-1} \to 0$ is taken, it is implied that the limit $Q \to \infty$ is taken first.

[35] Unlike the previous section, parameters $\tilde{\eta}$ and $\Omega^{-1}$ collapse to such single parameter $\nu$ only up to second order in $\nu$. At higher orders, terms are multiplied by an additional $\Omega^{-2}$.